JOURNAL OF PROPULSION AND POWER
Vol. 13, No. 3, May–June 1997

Modeling and Experiments of Laser-Induced Ignition of Nitramine Propellants

S. J. Ritchie,* S. T. Thynell,† and K. K. Kuo‡
Pennsylvania State University, University Park, Pennsylvania 16802

The objective of the work is to develop and experimentally verify a model for CO_2 laser-induced ignition of nitramine-based propellants. The one-dimensional model considers heat conduction in the condensed-phase coupled to heat and mass transport with global chemical kinetics of a heterogeneous propellant in the gas-phase region. The highly nonlinear model was solved numerically. Experimentally, increases in heat flux [125–375 W/cm^2 (193–578 cal/s-in.^{2})] lowered the ignition delay time, but changes in pressure [1.38–3.79 MPa (200–550 psia)] had very little effect. This supports the assumption that cyclotrimethylenetrinitramine decomposition is primarily temperature controlled. These trends are correctly predicted by the model. Predictions of ignition delay time match the experimental data within the measurement uncertainty. Sensitivities of the numerical solution to the material properties and kinetic rate constants are addressed.

Nomenclature

c = specific heat
D = diffusion coefficient
E = activation energy
k = rate constant
MW = molecular weight
P = pressure
$\dot{q}''$ = heat flux
$\dot{q}'''$ = volumetric heat release rate
R_u = gas constant
T = temperature
t = time
v = velocity
$\dot{w}''$ = species flux
$\dot{w}'''$ = volumetric species production rate
Y = species mass fraction
y = vertical coordinate in the direction outward from the propellant surface
α = thermal diffusivity
β = extinction coefficient
λ = thermal conductivity
ρ = density
σ = absorptivity of gas–solid interface

Subscripts
g = gas
j = jth species
LE = light emission
m = mixture
ref = reference value
reg = surface regression
s = solid

Presented as Paper 95-2862 at the AIAA/SAE/ASME/ASEE 31st Joint Propulsion Conference, San Diego, CA, July 10–12, 1995; received April 4, 1996; revision received Feb. 10, 1997; accepted for publication Feb. 17, 1997.

*Ph.D. Candidate, Department of Mechanical Engineering; currently Senior Process Engineer, Alliant Techsystems, Inc., Radford Army Ammunition Plant, Radford, VA 24141.

†Associate Professor, Department of Mechanical Engineering. Member AIAA.

‡Distinguished Professor and Director of the High-Pressure Combustion Laboratory, Department of Mechanical Engineering. Fellow AIAA.

Introduction

RECENTLY, significant interest has been placed on the use of lasers as an ignition source for large-caliber ballistic systems.[1] With the use of lasers, primers could be completely eliminated, resulting in a decreased vulnerability, simplified ignition train, and usage of insensitive ammunitions that are, by design, very difficult to ignite. Furthermore, by proper positioning of the laser or by using multiple lasers, a more uniform flame-spreading event is anticipated, thus reducing detrimental pressure gradients within the gun chamber. Based on these considerations it is highly beneficial to undertake fundamental studies that are focused on the ignition event; that is, the specific time interval over the power from the laser beam pyrolyzes the highly energetic material.

The ignition of materials through a radiative heating mechanism offers several advantages over other mechanisms. These include 1) the environmental parameters such as ambient gas composition, initial temperatures, and chamber pressure that can be varied independently of the incident heat flux and 2) incident flux levels and exposure intervals to the propellant surface that can be controlled very precisely. Numerous examples of laser-ignition studies are available in the literature. The pioneers in the use of radiative techniques for the study of solid propellant and fuel ignition characteristics were Ohlemiller and Summerfield[2] and Ohlemiller et al.[3] Early investigations on laser-induced ignition of polymeric materials were performed.[2,3] DeLuca et al.[4,5] conducted studies on double-base propellants by considering the effects of propellant formulation, inert heating, and the type of irradiation. Kashiwagi studied the effects of gas-phase attenuation on the surface temperature required for ignition.[6] The radiative source for these types of studies is typically either an arc-image furnace or a CO_2 laser. Ohlemiller and Summerfield[7] in a comparative study found that laser ignition offered several advantages over the arc-image furnace and the high-power CO_2 laser has become the standard source for radiative heating studies of solid propellant.

More recently, these techniques are being applied to low-vulnerability ammunition propellants (LOVA). Of particular interest to this program are the propellant candidates that contain cyclotrimethylenetrinitramine (RDX). A review of the open literature reveals very little work in this area. Kuo et al.[8]

have examined the preignition dynamics of RDX mixed with glycidyl azide polymer (GAP) binder and the energetic plasticizers TMETN and BTTN using a CO_2 laser. They measured ignition delay times and carried out species measurements above the propellant at ambient pressure. Five distinct gas-phase zones were identified during the ignition process. As part of the U.S. Army's laser initiation development program, Cohen and Beyer[9] and Cohen et al.[10] have carried out some modeling and laser ignition experiments of solid propellants.

The gas-phase ignition kinetics of pure RDX have been modeled by Melius[11] using a very comprehensive set of elementary reactions, but a distinct condensed phase was not considered in the model. Since the decomposition kinetics of the binders and plasticizers of interest to the LOVA program are not well known, a much simpler chemical kinetic scheme was more appropriate for this work. The approach taken is very similar to the recent work of Huang et al.,[12] where the ignition of two RDX-based propellants subjected to conductive heating via hot fragments was studied both experimentally and theoretically. The attractiveness of using this scheme lies not only in its relative simplicity but also in the opportunity to apply a similar global chemical scheme to different ignition scenarios.

The objective of this paper is to describe a model for laser-induced ignition of an RDX-based composite propellant, to summarize the experimental facility for acquiring data on ignition delay times, to discuss results obtained from a numerical solution with those obtained from experiments, and to propose areas in need of further work.

Experimental Approach

Test Facility

The CO_2 laser facility has been extensively used to study the problem of solid-propellant ignition and the details of this facility have been documented.[13–15] Thus, only a brief summary of the test setup shown in Fig. 1 is warranted. A Coherent Super 48 high-power CO_2 laser, capable of generating 800 W (191 cal/s) in the continuous wave mode and 3500 W (836.5 cal/s) in the pulsed mode, is used as the radiative source. To ensure a uniform flux over the sample surface a mask is used to block off all but a 0.7-cm- (0.3-in.-) diam circular portion of the laser beam output. The unhindered beam exhibits a Gaussian intensity profile that is relatively uniform across the sample surface with losses of 10–15% near the edges. Incident heat flux to the sample surface is measured separately by placing a calorimeter and an instrument for calibrating lasing time and beam intensity profile in the sample location.[16]

To obtain a reasonably wide pressure range, a high-pressure test chamber capable of withstanding 34.5 MPa (5000 psia) was used.[17] Two long, narrow Plexiglas® windows, located on the front and back faces of the chamber, as shown in Fig. 1, provide optical access for high-speed filming. A zinc selenide window, protected from combustion products by a potassium chloride window, allows for passage of the CO_2 laser beam.

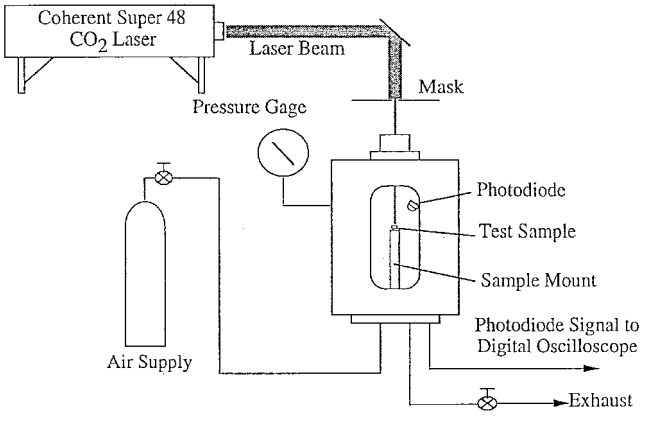

Fig. 1 Schematic diagram of the CO_2 laser ignition test facility.

The sample was positioned on a mounting plate and inserted through the bottom of the chamber. Variation of the ambient gas concentration is possible, but air was used for all tests described here. Experiments were carried out at pressures of 1.38 and 3.79 MPa (200–550 psia). Heat flux levels were between 125–375 W/cm^2 (193–578 cal/s-in.^{2}). Pretest pressure measurements were made using a dial gauge mounted directly on the chamber. Changes in pressure were negligible throughout the test because of the relatively large chamber volume (956 cm^3/58.3 in.^{3}).

Ignition delay time was measured using a silicon photodiode positioned inside the test chamber. The diode senses light emission in the visible wavelength range (0.35–1.15 μm) with a peak sensitivity at 0.9 μm. Data from this diode were stored on a digital oscilloscope, which was triggered by the firing of the laser. Post-test analysis identified the ignition delay time by finding the time at which the photodiode signal was three times greater than the average background level.

Propellant Description

XM39 solid propellant contains RDX crystalline particles (76% by weight) and an oxygenated fuel-rich binder. The binder ingredients are 12% cellulose acetate butyrate (CAB), 7.6% acetyl triethyl citrate (ATEC), 4% nitrocellulose (NC), and 0.4% ethyl centralite (EC). NC is a common homogeneous propellant that is slightly fuel-rich. CAB and ATEC are oxygenated hydrocarbon-based fuel binder materials. EC is a stabilizer for the NC. Important material properties of XM39 are given as follows: density, 1.678 g/cm^3; specific heat, 0.2771 cal/g-K; and thermal conductivity (variations for numerical sensitivity study), 0.499, 0.374, and 0.250×10^{-3} cal/cm-s-K.

Experimental preparation required cutting the samples by hand with a razor blade. The propellant was received in stick form (0.7 cm diam × 10.2 cm length) and was cut into thin discs about 0.5 cm thick × 0.7 cm diam. The discs were glued onto a holder such that the incident radiation was upon the flat, freshly cut surface.

Theoretical Model Description

The one-dimensional ignition model development follows a form similar to Kashiwagi[18] for solid fuels, and also similar to Kumar and Hermance[19] for homogeneous solid propellants. The following set of major assumptions was introduced to simplify the analysis.

1) The ignition is transient and one dimensional. The incident laser heat flux was radially uniform and the effect of sample edges on the ignition process was ignored.

2) The RDX particle size for the XM39 propellant is nominally 5 μm diameter. The propellant with a high percentage (76%) of numerous small particles can be considered homogeneous.

3) The amount of gaseous mass increase because of propellant gasification is small, resulting in a negligible increase in ambient gas pressure.

4) The perfect gas law is applicable.

5) The thermal properties of the condensed phase are temperature independent.

6) Numerous studies in the literature have identified the existence of a liquid melt layer on the surface of burning XM39 propellant.[20,21] The melt layer ranges in thickness from 100 to 300 μm for steadily burning samples of XM39. The thickness observed was inversely proportional to pressure.[21] As pressure increases, the larger heat feedback to the propellant surface leads to a sharper thermal profile in the condensed-phase of the material and a corresponding reduction in the thermal penetration depth. Hence, a reduced thickness of the melt layer. Likewise, if heating rates are high enough and the time scales short enough, a significant melt layer should not form prior to the observed light emission in these tests. Therefore, the liquid melt has been neglected in the derivation of the model.

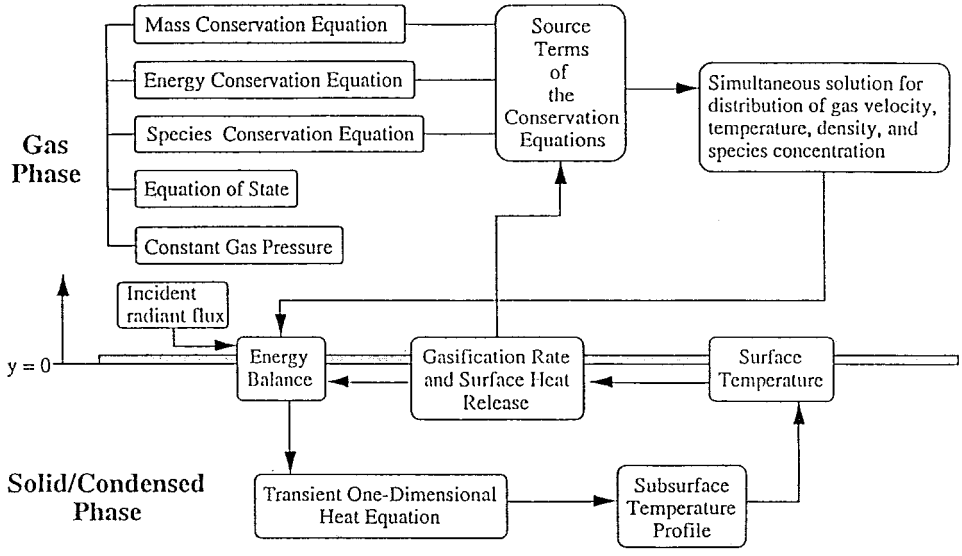

Fig. 2 Flowchart for the theoretical/numerical model for ignition of XM39 solid propellant.

7) The convective and diffusive forces dominate over the body forces that are neglected.

8) Although attenuation of the incident laser beam by gas-phase species can become very significant during steady-state combustion, experimental observation indicates that this effect is negligible during the ignition event. The radiative flux to the surface is therefore constant during the entire event.

9) To simplify the computational effort, the properties of air (c_p and λ) are used for all gases.

10) Diffusion coefficients for the gas-phase species are equal and calculated assuming a unit value of Lewis number.

11) The incident radiant energy is absorbed at the surface, with very little reflection or transmission indepth, because of the small crystalline size of RDX and highly absorptive behavior of CAB at the 10.6-μm wavelength of the CO_2 laser.

Governing Mathematical Equations

The physical configuration for the mathematical model is shown in Fig. 2. The position coordinate y is set equal to zero at the gas–solid interface with the positive direction into the gas phase. After incorporating the assumptions listed earlier, the ignition process can be represented by the set of mathematical equations listed in the figure and summarized as follows.

Solid-phase energy:

$$\rho_s c_s \left(\frac{\partial T}{\partial t} + v_{\text{reg}} \frac{\partial T}{\partial y} \right) = \lambda_s \frac{\partial^2 T}{\partial y^2} \tag{1}$$

Gas-phase continuity:

$$\frac{\partial \rho_g}{\partial t} + \frac{\partial \rho_g v_g}{\partial y} = 0 \tag{2}$$

Gas-phase equation of state:

$$P = \rho_g R_u T \sum_j \frac{Y_{j,g}}{MW_j} \tag{3}$$

Gas-phase energy:

$$\rho_g \frac{\partial (c_g T)}{\partial t} + \rho_g v_g \frac{\partial (c_g T)}{\partial y} = \frac{\partial}{\partial y} \left(\lambda_g \frac{\partial T}{\partial y} \right) + \dot{q}'''_g \tag{4}$$

Gas-phase species conservation:

$$\rho_g \frac{\partial Y_{j,g}}{\partial t} + \rho_g v_g \frac{\partial Y_{j,g}}{\partial y} = \frac{\partial}{\partial y} \left(\rho_g D_{j,m} \frac{\partial Y_{j,g}}{\partial y} \right) + \dot{w}'''_{j,g} \tag{5}$$

$$\sum_j Y_{j,g} = 1 \tag{6}$$

Initially, the gas-phase composition is air ($Y_{N_2} = 0.76$, $Y_{O_2} = 0.23$, and $Y_{Ar} = 0.01$). Even though the chemical model does not include these species, they are tracked because of their importance to the calculation of gas-phase density. Also, the temperatures of the gas- and solid-phases are initially equal at a standard temperature of 300 K. Both the gas and solid phases are treated as semi-infinite media. The following boundary conditions apply:

$$y \to -\infty \text{(solid-phase)}: \quad T = T_{s,\text{initial}} \tag{7}$$

$$y \to +\infty \text{(gas phase)}: \quad T = T_{g,\text{initial}} \quad \text{and} \quad Y_{j,g} = Y_{j,g,\text{initial}} \tag{8}$$

The two media are coupled at the interface ($y = 0$), where the boundary conditions are given by

$$T_g = T_s \tag{9}$$

$$\rho_g v_g = \rho_s v_{\text{reg}} \tag{10}$$

$$\rho_s v_{\text{reg}} Y_j \big|_{y=0-} = \rho_g v_g Y_j \big|_{y=0+} - \rho_g D_j \frac{\partial Y_{j,g}}{\partial y} - \dot{w}''_j \tag{11}$$

$$\left(\lambda_s \frac{\partial T}{\partial y} \right)_{y=0-} = \left(\lambda_g \frac{\partial T}{\partial y} \right)_{y=0+} + \rho_g v_g (c_s - c_g)(T_s - T_{\text{ref}}) + \sigma_s \dot{q}''_{\text{laser}} + \dot{q}''_{\text{reaction}} \tag{12}$$

The source terms for the energy and species equations depend on the assumed chemical kinetic mechanism of XM39 decomposition and ignition. The source term for the species in Eq. (11) is determined using the regression velocity. For example, to determine the mass generation of RDX

$$\dot{w}''_{\text{RDX}} = \rho_s v_{\text{reg}} Y_{\text{RDX},s} \tag{13}$$

The other species would be determined by finding the mass percentage of a solid ingredient and then breaking it down according to the chemical equations given next.

Chemical Kinetic Model of XM39

A comprehensive set of elementary chemical reactions of RDX combustion has been developed by Melius.[22] To couple such a scheme with a condensed-phase region could become computationally very intensive. Furthermore, since the binder decomposition kinetics has not been determined experimentally, a compromise in the chemical kinetic model must be sought. Huang et al.[12] have identified a set of reactions that successfully predicted the go/no-go ignition boundaries for two nitramine-based propellants, including XM39. The major chemical steps in the model are as follows:

$$\mathrm{RDX(s)} \rightarrow \mathrm{RDX(g)} \tag{R1}$$

$$\mathrm{ATEC:\ C_{14}H_{22}O_8(s) \rightarrow 5CH_2O(g) + 3C_2H_4(g) + 3CO(g)} \tag{R2}$$

$$\mathrm{NC:\ C_6H_8O_5(NO_2)_{2.45}(s) \rightarrow 2.45NO_2(g) + 2CH_2O(g) + 2CO(g) + C_2H_2(g) + H_2O(g)} \tag{R3}$$

$$\mathrm{CAB:\ C_{15}H_{22}O_8(s) \rightarrow 6CH_2O(g) + 3C_2H_2(g) + CH_4(g) + 2CO(g)} \tag{R4}$$

$$\mathrm{RDX(g) \rightarrow 3CH_2O(g) + 3N_2O(g)} \tag{R5}$$

$$\mathrm{RDX(g) \rightarrow 3HCN(g) + 3/2NO(g) + 3/2NO_2(g) + 3/2H_2O(g)} \tag{R6}$$

$$\mathrm{NO_2(g) + 5/7CH_2O(g) \rightarrow NO(g) + 3/7CO(g) + 2/7CO_2(g) + 5/7H_2O(g)} \tag{R7}$$

The kinetic rate constants, shown in Table 1, provide very good agreement with the hot fragment conductive ignition (HFCI) measurements of Huang et al.[12] In an effort to establish the accuracy of these rate constants, no effort was made to vary them as a means of fitting the experimental data. Second-order Arrhenius terms are used in the source term evaluation for all of the gas-phase reactions. From these seven reactions, there are 15 gas-phase species (Ar, RDX, CH_2O, N_2O, NO, NO_2, HCN, H_2O, CO, CO_2, C_2H_2, C_2H_4, CH_4, N_2, and O_2), whose concentrations must be tracked using the species conservation equations.

All of the individual components of the solid material follow separate decomposition paths as shown in reactions (R1–R4). Since decomposition of XM39 propellant in the condensed phase can be regarded as negligible, RDX enters the gas phase via a vaporization process (R1). In the gas-phase, RDX decomposition follows the two general pathways shown by reactions (R5) and (R6). Kinetic rates for these two pathways are based on first-order Arrhenius kinetics. At lower temperatures, reaction (R5) is favored and CH_2O and N_2O are predominantly formed. As the temperature increases, greater amounts of HCN and HONO are formed by reaction (R6). HONO is a relatively unstable species in this scheme and the decomposition to H_2O, NO, and NO_2 is assumed to occur very rapidly.

The binder constituents (NC, CAB, ATEC, and EC) are treated differently from RDX. The binder decomposition takes place at the gas–solid interface so that only products are considered in the gas phase (R2, R3, and R4). Assuming the mass fractions of the solid-phase species remain constant, the decomposition rate of the binders and the vaporization of RDX are governed by the regression rate of the propellant. The regression rate was governed by the following two equations based on the differential scanning calorimeter (DSC) measurements of Miller et al.[23] Equation (14) has a constant pre-exponential factor, but Eq. (15), which is a more accurate fit of the decomposition data, has a heating-rate-dependent pre-exponential factor

$$k_{\mathrm{reg}} = 1.98 \times 10^{14}(1/s)\exp(-E_{\mathrm{reg},1}/R_uT) \tag{14}$$

$$k_{\mathrm{reg}} = 7.79 \times 10^{17}\left(\frac{\mathrm{d}T}{\mathrm{d}t}\right)^{-0.516}\left(\frac{1}{s}\right)\exp\left(-\frac{E_{\mathrm{reg},2}}{R_uT}\right) \tag{15}$$

where $E_{\mathrm{reg},1}$ = 38.2 kcal/mol and $E_{\mathrm{reg},2}$ = 47.2 kcal/mol. The temperature in Eqs. (14) and (15) corresponds to the furnace temperature for a DSC and therefore represents both surface and in-depth degradation processes. Ohlemiller and Kashiwagi[24] have shown that, for solid polymeric fuels subjected to very low incident heat fluxes, the gasification rate changes significantly despite a constant value of surface temperature. The increase is attributed to an in-depth gasification process and the formation of bubbles beneath the surface. Therefore, the regression velocity was determined by applying the degradation kinetics over the entire solid-phase domain and then integrating to find the total mass loss. This amount was then applied at the surface of the solid to obtain a surface regression velocity. The influence of transport within the solid-phase was effectively ignored by assuming instantaneous movement of degradation products to the surface and into the gas-phase.

The effect of EC on the chemical reactivity was assumed to be negligible because of its small initial concentration in the XM39 formulation. Of the remaining binder constituents, only NC has been studied in great detail.[25,26] Because of the lack of detailed information, the decomposition mechanisms for the binder materials are based on a number of important general characteristics. First, the balanced decomposition mechanism should be endothermic. Second, decomposition products are chosen to match available data wherever possible and likely products are chosen where data are unavailable. For example, soot has been observed in the dark zone of the XM39 flame; therefore, soot precursors are considered in the CAB and ATEC mechanisms. Third, only stable products are considered in the mechanism. Radicals such as OH and O are highly reactive intermediate species that would be involved in very rapid chemical reactions that are not rate limiting.

In many instances, ambient oxygen can play an important role in the ignition delay time of XM39 propellants.[27,28] This occurs because of increased mixing[27] or low initial heat fluxes and pressures that allow for significant oxygen diffusion into the reaction zone from the ambient.[28] In cases where the oxygen is more effectively displaced by the decomposition gases, the oxygen influence is limited. In the radiative ignition sce-

Table 1 Chemical rate constants and heats of reaction for the chemical model

Reaction number	Arrhenius prefactor	Activation energy	Heat of reaction	Reference
R1	$7.79 \times 10^{17}(dT/dt)^{-0.516}$, 1/s[a]	47.2, kcal/gmol[a]	140, cal/g RDX	23
R2	$7.79 \times 10^{17}(dT/dt)^{-0.516}$, 1/s[a]	47.2, kcal/gmol[a]	−1870, cal/g ATEC	23
R3	$7.79 \times 10^{17}(dT/dt)^{-0.516}$, 1/s[a]	47.2, kcal/gmol[a]	277.7, cal/g NC	23
R4	$7.79 \times 10^{17}(dT/dt)^{-0.516}$, 1/s[a]	47.2, kcal/gmol[a]	955.6, cal/g CAB	23
R5	1×10^{13}, 1/s	36, kcal/gmol	−314.95, cal/g RDX	22
R6	2×10^{16}, 1/s	45, kcal/gmol	38.84, cal/g RDX	22
R7	1×10^{12}, cm^3/gmol s	19, kcal/gmol	−999.16, cal/g NO_2	29

[a]Rates governed by surface regression terms found in the text.

nario under study, the pressure and heat flux are both very high. High heat fluxes lead to high gasification rates at the surface that displace the ambient gases, such as oxygen. The high-pressure forces the decomposition gases close to the sample surface, where the larger concentrations and high temperatures lead to shorter reaction times. This reduces or precludes the influence of oxygen on the reaction scheme.

In the gas phase, reaction (R7) is generally accepted as a reasonable source of the gas-phase heat feedback from the primary flame zone.[29–31] In the reaction scheme considered in the present model, this reaction is quite important in providing exothermic heat release during the ignition process. The amount of heat released by this reaction can significantly increase the gas-phase temperature adjacent to the propellant surface, leading to conductive heat feedback. This time was determined by tracking the concentration of the product species. Significant increases in reactivity were observed when the mass fraction of CO_2 exceeded a critical value of 0.0055; therefore, this was used as the ignition criterion. The ignition delay time sensitivity of the product species (CO_2) based ignition criterion was examined by varying the mass fraction critical level from 0.0055 to 0.1. The change in the predicted ignition delay time was 1.2%. Because there is a very sharp increase in the products as reaction (R7) rapidly increases the temperature and consumes the reactant species, there is only a small change in the ignition delay time. It would, therefore, be reasonable to have chosen a critical mass fraction anywhere in the studied range without introducing significant variation or error.

Ideally, the choice of ignition criterion should closely match the one used in the experimental program. Unfortunately, the evaluation of light emission is not provided for in the model. This could introduce some error in the comparison of the model to experiment. In models for steady-state combustion of these propellants, the previous chemistry is often associated with the primary flame zone, not the secondary luminous flame zone. Therefore, the luminosity of the flame is not ordinarily associated with the chemistry chosen. It may be argued though that the luminosity observed in the experiment could arise from the CO chemiluminescence that would be associated with the CO formation in reaction (R7). If this is the case, there could be a direct linkage between the model and experiment with respect to the ignition delay time.

Method of Solution

To start the numerical solution an initial guess of the surface temperature was required. This temperature was used to determine the gasification rate of the propellant. The gasification rate was required for the source terms in the gas-phase conservation equations. In the gas phase, the mass and energy conservation equations, 15 species conservation equations, and an equation of state were solved simultaneously at all grid points. The obtained profiles were used to carry out an energy balance at the surface that was used as a boundary condition to solve the one-dimensional heat equation of the solid for the solid-phase temperature profile. The surface temperature from this solution was compared to the initial guess. If necessary, the initial guess was adjusted and the previous process repeated until convergence. Once convergence was reached, the time was increased by one time step and the previous process was repeated. To facilitate computational solution, the gas and solid phases were discretized using stretched grids. Second-order-accurate central differencing was used for all derivatives, and a Crank–Nicolson scheme was employed to solve the resulting equations. To ensure the solution was not grid or time-step dependent, the number of grid points and the time steps were varied until no changes in the converged values were observed. The material properties utilized in the computation are shown in Table 1.

Results and Discussion

Model Results

In this section, the results of the theoretical predictions are discussed and compared with the experimental data. To provide detailed information on the predictive capability of the proposed model, the results of a typical ignition problem are presented first by considering P = 2.07 MPa, $\dot{q}''_{laser}$ = 300 W/cm^2, and $\alpha_s = 0.80 \times 10^{-3}$ cm^2/s. The incident radiative flux is applied for all $t \geq 0^+$.

Figure 3 shows the predicted temperature profiles at selected time intervals. The interface between the solid and gas is located at $y = 0$ and represented by the vertical solid line; negative values of position are in the solid and positive values are in the gas phase. Up to t = 2 ms, the profiles are characteristic of inert heating with conductive losses to the gas and solid phases. The effects of gas-phase reactions are recognized after 3 ms. Within the gas phase, the temperature begins to rise because of the heat release from the exothermic reactions (R5 and R7), which release energy faster than required for the endothermic reaction (R6). As the gas temperature rises above the surface temperature, conductive heat feedback from the reaction zone increases the gasification process. At 4.04 ms, the ignition criterion has been met at a position approximately 0.015 cm from the sample surface and the simulation is stopped. Following this time, the chemical reactions proceed at a rapidly accelerating rate.

The reaction zone is best shown using plots of the various species that are tracked in the gas phase. Figure 4 describes the predicted RDX mass fraction as a function of position and time. At the surface ($y = 0$) the mass fraction is determined by the gasification rate of the propellant. It rises from Y_{RDX} = 0 at $t = 0$ to Y_{RDX} = 0.76 at the end of the simulation. Until the ignition time, the gasified RDX is carried away from the surface via convective and diffusive processes without any significant decomposition. At t = 4.04 ms there is a sharp drop in the concentration of the RDX near y = 0.015 cm. If the code continued to execute, the gaseous RDX would rapidly be depleted and the reaction zone would widen.

The major decomposition products of RDX, which are important for simulating gas-phase ignition, are CH_2O and NO_2. The mass fractions as a function of position and time are shown for these two species in Figs. 5 and 6, respectively. The mass fraction of CH_2O and NO_2 at the surface is because of the decomposition of binder species (CAB, ATEC, and NC).

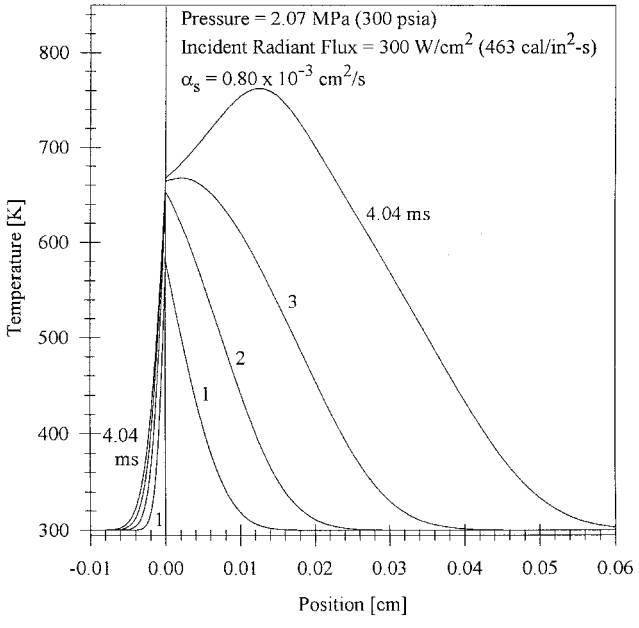

Fig. 3 Model predictions of solid- and gas-phase temperature profiles at various times for typical test conditions.

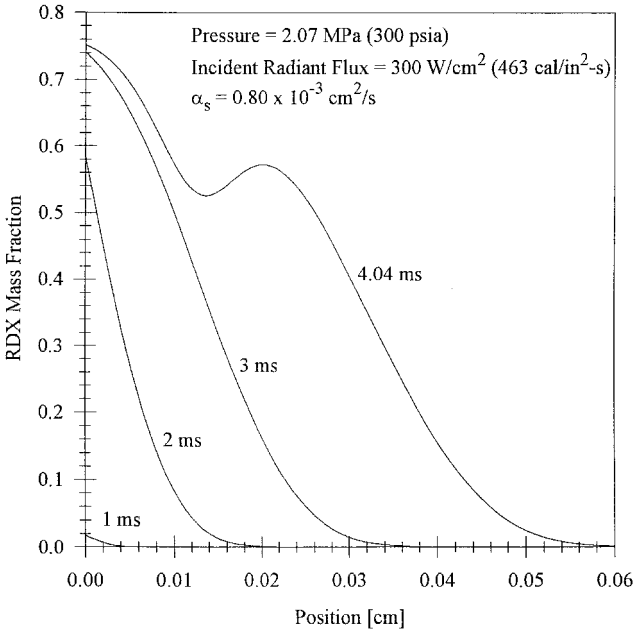

Fig. 4 Model predictions of the gas-phase RDX mass fraction profile at various times.

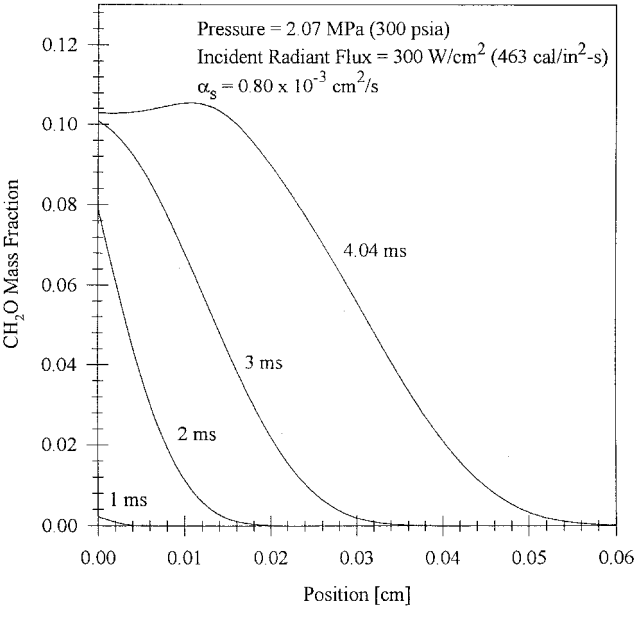

Fig. 5 Model predictions of the gas-phase CH_2O mass fraction profile at various times.

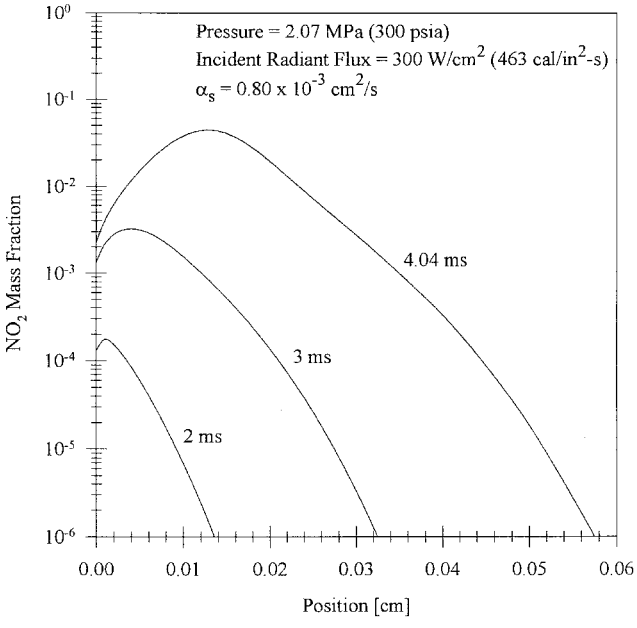

Fig. 6 Model predictions of the gas-phase NO_2 mass fraction profile at various times.

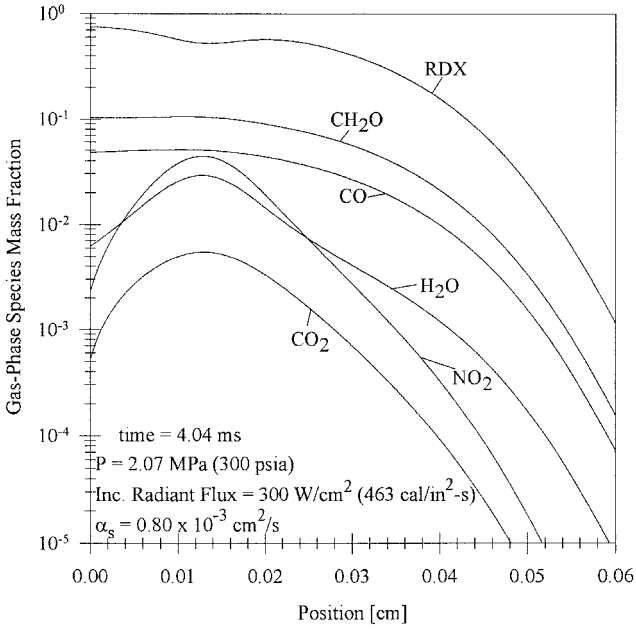

Fig. 7 Selected gas-phase species mass fraction profiles at the ignition time.

Until ignition, the behavior of CH_2O is similar to the behavior of RDX. The mass fraction in the gas phase increases with increasing distance from the surface because of diffusion, convection, and RDX decomposition. At ignition, there is a slight increase in the gas-phase composition of CH_2O because of the increasing rate of decomposition of RDX. A greater increase would be expected if ignition was delayed, but CH_2O is rapidly consumed from exothermic reactions with NO_2, and thus, less CH_2O exists during continued RDX decomposition. A second reason for lower values of CH_2O is because of the reaction (R6), which becomes more important for temperatures above 600 K.

The NO_2 mass fraction behaves somewhat differently compared to CH_2O. There is only a small amount of NO_2 generated at the surface by the decomposition of the binder. The majority of it is formed via the breakdown of RDX in the gas-phase region. This can be seen in Fig. 6, which presents the NO_2 mass fraction profiles at selected time intervals. The maximum concentration of NO_2 does not occur at the surface but is located in the gas-phase region. Again, the decomposition path for RDX that produces HONO and HCN (with rapid removal of HONO to form NO, NO_2, and H_2O) becomes more dominant at temperatures above 600 K. Therefore, for temperatures above 600 K the concentration of NO_2 increases rather dramatically.

Figure 7 shows the concentration as a function of position for six major gas-phase species at the ignition. It is obvious from this plot that the location of maximum reactivity is 0.015 cm above the surface of the sample. All major product species, as well as NO_2, show a significant increase at this location; whereas the RDX concentration drops because of its decomposition. The increase of NO_2 and CH_2O is tempered by further reactions to the final products of reaction (R7). Results similar to these were found for all of the test runs. The differences were observed in the location of the reaction zone and the time required to reach the ignition threshold.

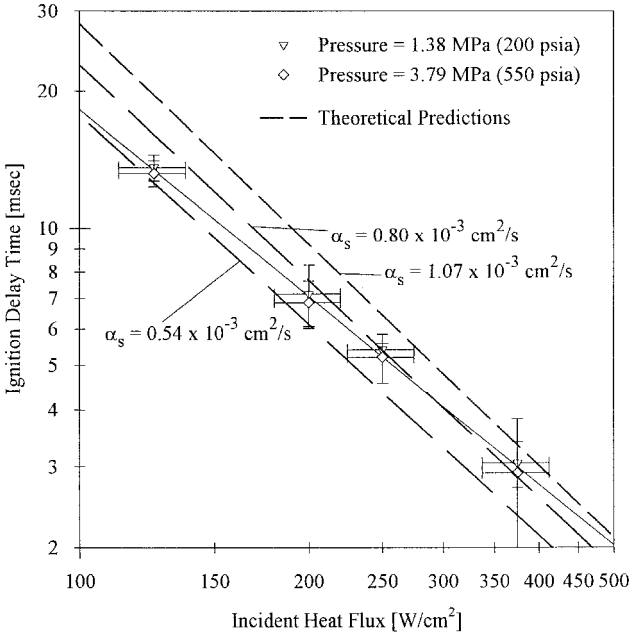

Fig. 8 Comparison of experimental results to model predictions using three different values for thermal diffusivity.

Effect of Changes in Incident Heat Flux

As expected, there is a strong effect of incident heat flux on the measured light emission delay time. This trend is successfully captured in the model as well. Figure 8 illustrates the ignition delay time (or light emission time) vs the incident heat flux. Experimental results are shown as data points. The vertical error bars represent the standard deviation of the averaged test results (three to five tests for each point). The horizontal error bars represent the uncertainty in the determination of the experimental incident flux levels. Data taken at two separate pressures are indicated, but there was very little effect of pressure on observed light emission times in the range studied. The line of best fit through all of the experimental data is given by

$$\frac{t_{LE}}{t_{LE,ref}} = \left(\frac{\dot{q}''_{laser,ref}}{\dot{q}''_{laser}} \right)^{1.37} \tag{16}$$

where $t_{LE,ref}$ = 13.08 ms and $\dot{q}''_{laser,ref}$ = 125 W/cm^2 (193 cal/s-in.^{2}).

The dashed lines are the model predictions for different values of thermal diffusivity, as indicated. These values were achieved by changing the code input of the thermal conductivity. This shows the sensitivity of the numerical results to changes in the thermal properties of the solid propellant. The slopes of the predicted lines are steeper than that of the measured data. For the higher flux levels, larger values of thermal diffusivity predict the ignition delay time. As the flux level is reduced the predictions using the large values for thermal diffusivity deviate further from the experimental observation. Ignition delay times were predicted more closely using lower thermal diffusivity values for lower incident heat fluxes.

It is well accepted that the thermal transport properties of propellants are functions of temperature. These changes could easily describe the discrepancy observed between the experimental data and the predicted results from the model, which assumes a constant value for the thermal properties of the solid throughout the ignition transient. The present form of the model could be improved by relaxing this assumption. Other parameters that are not well known but have a strong influence on the predicted results include the gasification and chemical kinetic rate constants. Further analysis of these factors should be carried out as discussed in the Conclusions section.

Pressure Effect

As can be seen in Fig. 8, changes in pressure had very little effect on the measured ignition delay time. This was also the case with the numerical model. As pressure decreased, the location of the ignition site moved further from the propellant surface, but this did not significantly alter the ignition delay time until the pressure was well below the range studied. This is in agreement with expectations. It is well accepted that decreases in pressure increase the blowing velocity effect and reduce the collision frequency, as well as the chemical reaction rates, thus moving the reaction zone away from the propellant surface. As the exothermic reaction zone moves away from the surface, the heat feedback decreases resulting in longer ignition delay times. The opposite is true for higher pressure situations. However, eventually a limiting case must be reached where further increases in pressure result in negligible reductions in the delay time. The limited importance of pressure tends to support the assumption of unimolecular decomposition of RDX, which is assumed to be dependent upon temperature alone.

Conclusions

Experimentally measured ignition delay time data for a nitramine-based composite propellant (XM39) have been compared to predictions made with a gas-phase ignition model that relies on a simplified chemical kinetic scheme. Experimentally, increases in heat flux lowered the light emission or ignition delay time, but changes in pressure, within the range studied, at a given incident flux had very little effect. This supports the assumption that RDX decomposition is primarily temperature controlled. These trends are correctly predicted by the model. Actual prediction of the ignition delay time is in reasonably good agreement with experiments, within the constraints of the assumptions used to formulate the model. As shown in the calculated results with different values of thermal diffusivity of the solid propellant, ignition delay time could be affected by the physical properties, which are characterized only at lower temperatures ($-40°C < T < 50°C$). More detailed information on radiative absorption properties and gasification rate constants could also improve model predictability.

Further improvements to the model can be made. First, as more information becomes available about the decomposition kinetics of the binder ingredients, in particular CAB and ATEC, their global decomposition mechanisms should be modified. The sensitivity of the ignition delay time to the kinetic constants used in the present model was not studied because the objective was to use representative values from the literature. Second, the effect of a foam layer and its influence on the properties of the propellant surface should be considered, including a two-phase region with a limited role of decomposition kinetics. The effects of a foam layer could be very important if other solid propellants are to be studied, including those containing energetic plasticizers and other cyclic nitramines. Third, the functional variation of material properties such as thermal conductivity and specific heat with temperature should be incorporated along with the in-depth absorption characteristics as greater understanding of the material is achieved. For example, in-depth absorption would tend to increase the thermal penetration depth that would result in a lower gasification rate and a longer ignition delay time for a given condition. However, the magnitude of this difference may be very small depending on the amount and extent of the in-depth energy absorption.

Acknowledgments

This work was performed, in part, under Grant DAAL-03-92-G-0020 with the U.S. Army Research Office, Research Triangle Park, North Carolina. The support and encouragement of the program manager, D. M. Mann, are gratefully acknowledged. The authors would also like to acknowledge the support

and interest of J. Heimerl of the U.S. Army Research Laboratory.

References

[1]Barrows, A. W., Forch, B. E., Beyer, R. A., Cohen, A., and Newberry, J. E., "Laser Ignition in Guns, Howitzers and Tanks: The LIGHT Program," *28th JANNAF Combustion Meeting*, Chemical Propulsion Information Agency, Publ. 573, Vol. 1, 1991, pp. 441–451.

[2]Ohlemiller, T. J., and Summerfield, M., "Radiative Ignition of Polymeric Materials in Oxygen-Nitrogen Mixtures," *13th Symposium (International) on Combustion*, The Combustion Inst., Pittsburgh, PA, 1971, pp. 1087–1094.

[3]Ohlemiller, T. J., Caveny, L. H., DeLuca, L., and Summerfield, M., "Dynamic Effects on Ignitability Limits of Solid Propellants Subjected to Radiative Heating," *14th Symposium (International) on Combustion*, The Combustion Inst., Pittsburgh, PA, 1973, pp. 1297–1307.

[4]DeLuca, L., Caveny, L. H., Ohlemiller, T. J., and Summerfield, M., "Radiative Ignition of Double-Base Propellants: I. Some Formulation Effects," *AIAA Journal*, Vol. 14, No. 7, 1976, pp. 940–946.

[5]DeLuca, L., Ohlemiller, T. J., Caveny, L. H., and Summerfield, M., "Radiative Ignition of Double-Base Propellants: II. Pre-Ignition Events and Source Effects," *AIAA Journal*, Vol. 14, No. 8, 1976, pp. 1111–1117.

[6]Kashiwagi, T., "Effects of Attenuation of Radiation on Surface Temperature for Radiative Ignition," *Combustion Science and Technology*, Vol. 20, Nos. 3, 4, 1979, pp. 225–234.

[7]Ohlemiller, T. J., and Summerfield, M., *AIAA Journal*, Vol. 6, No. 5, 1968, pp. 878–886.

[8]Kuo, K. K., Kim, J. U., Fetherolf, B. L., and Torikai, T., "Preignition Dynamics of RDX-Based Energetic Materials Under CO_2 Laser Heating," *Combustion and Flame*, Vol. 95, No. 4, 1993, pp. 351–361.

[9]Cohen, A., and Beyer, R. A., "Modeling Laser Ignition of Propellants: I. Ignition Delays," *28th JANNAF Combustion Meeting*, Combustion Propulsion Information Agency, Publ. 573, Vol. 1, 1991, pp. 435–440.

[10]Cohen, A., Beyer, R. A., Bilyk, S. R., and Newberry, J. E., "Laser Ignition of Solid Propellants: Comparison of Model Predictions with Emission and Pressure Measurements," *29th JANNAF Combustion Meeting*, Combustion Propulsion Information Agency, Publ. 593, Vol. 1, 1992, pp. 123–128.

[11]Melius, C. F., "Theoretical Studies of the Chemical Reactions Involved in the Ignition of Nitramines," *24th JANNAF Combustion Meeting*, Combustion Propulsion Information Agency, Publ. 476, Vol. 1, 1987, pp. 359–366.

[12]Huang, T. H., Thynell, S. T., and Kuo, K. K., "Hot Fragment Conductive Ignition of Nitramine-Based Propellants," *Journal of Propulsion and Power*, Vol. 11, No. 4, 1995, pp. 781–790.

[13]Chen, D. M., "Pyrolysis, Ignition and Combustion of Solid Fuels for Ramjet Applications," Ph.D. Dissertation, Dept. of Materials Science and Engineering, Pennsylvania State Univ., Univ. Park, PA, 1988.

[14]Chen, D. M., Hsieh, W. H., Snyder, T. S., Yang, V., Litzinger, T. A., and Kuo, K. K., "Combustion Behavior and Thermophysical Properties of Metal-Based Solid Fuels," *Journal of Propulsion and Power*, Vol. 7, No. 2, 1991, pp. 250–257.

[15]Kim, J. U., "Laser Ignition of Nitramine Composite Propellants," Ph.D. Dissertation, Dept. of Mechanical Engineering, Pennsylvania State Univ., University Park, PA, 1988.

[16]Fetherolf, B. L., Litzinger, T. A., and Kuo, K. K., "An Instrument for Measuring High-Power Laser Beam Profiles and Beam Attenuations," *Review of Scientific Instruments*, Vol. 61, No. 1, 1990, pp. 7–10.

[17]Kuo, K. K., Andiroglu, E., and Kamath, H., "Development and Design of a Laser Ignition Test Chamber," Final Rept. to the Ignition Devices Div., Naval Ordinance Station, Indian Head, MD, 1982.

[18]Kashiwagi, T., "A Radiative Ignition Model of a Solid Fuel," *Combustion Science and Technology*, Vol. 8, Nos. 5, 6, 1974, pp. 225–236.

[19]Kumar, R. K., and Hermance, C. E., "Role of Gas Phase Reactions During Radiant Ignition of Solid Propellants," *Combustion Science and Technology*, Vol. 14, Nos. 4–6, 1976, pp. 169–175.

[20]Schroeder, M. A., Fifer, R. A., Miller, M. S., Pesce-Rodriquez, R. A., and Singh, G., "Condensed-Phase Processes During Solid Propellant Combustion. Part II: Chemical and Microscopic Examination of Conductively Quenched Samples of RDX, XM39, JA2, M30, and HMX-Binder Compositions," Ballistic Research Lab., TR-337, Aberdeen Proving Ground, MD, 1992.

[21]Wilson, S. J., Fetherolf, B. L., Brown, P. W., and Kuo, K. K., "Surface Microstructure Resulting from Laser-Induced Pyrolysis and Combustion of M43 and XM39," Combustion Propulsion Information Agency, Publ. 606, Vol. 2, 1993, pp. 167–182.

[22]Melius, C. F., "Thermochemical Modeling: I. Application to Decomposition of Energetic Materials," *Chemistry and Physics of Energetic Materials*, edited by S. Bulusu, Kluwer Academic, Dordecht, The Netherlands, 1990, pp. 51–78.

[23]Miller, M. S., Kotlar, A. J., Cohen, A., Puckett, D. L., Holmes, H. E., and Troung, K., "Effective Ignition Kinetics for LOVA Propellant," Ballistic Research Lab., MR-3724, Aberdeen Proving Ground, MD, 1988.

[24]Kashiwagi, T., and Ohlemiller, T. J., "A Study of Oxygen Effects on Nonflaming Transient Gasification of PMMA and PE During Thermal Irradiation," *19th Symposium (International) on Combustion*, The Combustion Inst., Pittsburgh, PA, 1982, pp. 815–823.

[25]Schroeder, M. A., "Critical Analysis of Nitramine Decomposition Data: Product Distributions from HMX and RDX Decomposition," Ballistic Research Lab., TR-265, Aberdeen Proving Ground, MD, 1985.

[26]Fifer, R. A., "Chemistry of Nitrate Ester and Nitramine Propellants," *Fundamentals of Solid Propellant Combustion*, edited by K. K. Kuo, and M. Summerfield, Vol. 90, Progress in Astronautics and Aeronautics, AIAA, Washington, DC, 1984, pp. 177–238.

[27]Ritchie, S. J., Hsieh, W.-H., and Kuo, K. K., "Ignition of RDX-Based Solid Propellant Subjected to Crossflow Convective Heating," *Journal of Propulsion and Power*, Vol. 8, No. 3, 1992, pp. 570–577.

[28]Chang, L. M., and Rocchio, J. J., "Simulator Diagnostics of the Early Phase Ignition Phenomena in a 105-mm Tank Gun Chamber," Ballistic Research Lab., TR-2890, Aberdeen Proving Ground, MD, 1988.

[29]BenReuven, M., and Summerfield, M., "Combustion of Nitramine Propellants," Army Ballistic Research Lab., CR-00507, Aberdeen Proving Ground, MD, 1983.

[30]BenReuven, M., Caveny, L. H., Vichnevetsky, R. J., and Summerfield, M., "Flame Zone and Sub-Surface Reaction Model for Deflagrating RDX," *16th Symposium (International) on Combustion*, The Combustion Inst., Pittsburgh, PA, 1976, pp. 1223–1233.

[31]Oyumi, Y., and Brill, T. B., "Thermal Decomposition of Energetic Materials 3. A High-Rate, In Situ, FTIR Study of the Thermolysis of RDX and HMX with Pressure and Heating Rate as Variables," *Combustion and Flame*, Vol. 62, No. 3, 1985, pp. 213–224.